Increasing the Curie temperature of Ca_2FeMoO_6 double perovskite by introducing near-neighbour antiferromagnetic interactions

2005 J. Phys.: Condens. Matter 17 8037

(http://iopscience.iop.org/0953-8984/17/50/021)

INSTITUTE OF PHYSICS PUBLISHING JOURNAL OF PHYSICS: CONDENSED MATTER

J. Phys.: Condens. Matter **17** (2005) 8037–8047 doi:10.1088/0953-8984/17/50/021

Increasing the Curie temperature of Ca_2FeMoO_6 double perovskite by introducing near-neighbour antiferromagnetic interactions

D Rubi[1], C Frontera[1], A Roig[1], J Nogués[2], J S Muñoz[3] and J Fontcuberta[1]

[1] Institut de Ciència de Materials de Barcelona, CSIC, Campus UAB, 08193, Bellaterra, Spain
[2] Institut Català de Recerca i Estudis Avançats (ICREA), 08193, Bellaterra, Catalunya, Spain
[3] Departament de Física, Universitat Autònoma de Barcelona, 08193, Bellaterra, Catalunya, Spain

Received 24 August 2005, in final form 19 October 2005
Published 2 December 2005
Online at stacks.iop.org/JPhysCM/17/8037

Abstract

We report on the magnetic, magnetotransport and structural characterization of $(Ca_{1-y}Nd_y)_2Fe_{1+x}Mo_{1-x}O_6$ ($x < 0.5$) ferromagnetic double perovskites. It is found that the presence of an excess ($x > 0$) of Fe ions in the metallic sublattice produces a remarkable increase, by more than 90 K, of the Curie temperature. Mössbauer spectroscopy data indicate a reinforcement of the magnetic interactions. We argue that this dramatic enhancement of the ferromagnetic order is due to the strong antiferromagnetic superexchange coupling between near-neighbour Fe–Fe occupying regular and antisite positions in the structure. Moreover, the results indicate that the excess of magnetic ions (Fe) is essential to overcome the dilution effects caused by antisite defects.

1. Introduction

Ferromagnetic double perovskites of the type A_2FeMoO_6 (A = Ca, Sr, Ba) have been extensively studied in the past years, due to their high Curie temperature and half-metallic character [1], which makes them very promising candidates for the development of spintronic devices. The ideal cationic arrangement in this structure is an ordered Fe–Mo–Fe sequence along each axis of the perovskite unit cell. This naturally defines two sublattices at the B site of the perovskite: one is occupied by Fe and the other by Mo ions. Conduction electrons (spin-down), shared between hybridized 3d(Fe) and 4d(Mo) orbitals, are thought to be antiferromagnetically coupled to localized Fe magnetic moments (spin-up with $S = 5/2$) [2], and play a key role in the stabilization of the ferromagnetic state, in a mechanism that resembles the double exchange interaction. Kanamori *et al* [3] and Tovar *et al* [2] proposed that the Curie temperature of double perovskites is related to the density of states at the Fermi level ($D(E_F)$), and thus electron doping appeared as a natural strategy to modify their Curie temperature (T_C). Indeed, it was shown that replacing the divalent A^{2+} cation by a trivalent lanthanide

(La^{3+}, Nd^{3+}) in A_2FeMoO_6 promotes a substantial rise of the Curie temperature [4–11]. Subsequent photoemission experiments [12] experimentally confirmed the existence of a close correlation between T_C and $D(E_F)$.

Experimentally, the order between Fe and Mo ions is not perfect. This means that a certain fraction of Mo ions are placed at the Fe sublattice and vice versa. These misplaced ions are called antisites. The impact of antisite defects on the magnetic coupling of double perovskites has been controversial. Early Monte Carlo simulations by Ogale *et al* [13], and more recently by Frontera *et al* [14], have predicted that the Curie temperature decreases monotonically on increasing the cationic disorder. However, mean field calculations by Alonso *et al* [15] suggested that a moderate amount (up to 10%) of antisite defects could lead to an increase of the Curie temperature of Sr_2FeMoO_6. These authors argued that this effect could result from the strong $3d^5$–$3d^5$ Fe–Fe nearest-neighbour interactions between Fe ions at regular and irregular (antisite) positions, that, owing to their superexchange nature, should be strongly antiferromagnetic (AFM). Therefore, the ferromagnetic order of next-nearest-neighbour Fe ions in Mo–Fe–Fe–Fe–Mo arrangements should be enhanced [15]. A similar mechanism was also proposed by Solovyev [16].

However, in contrast with these predictions, it was experimentally shown that this type of cationic disorder unambiguously reduces the Curie temperature of Sr_2FeMoO_6 [17]. A plausible explanation for this effect arises from the fact that the existence of antisites implies the presence of non-magnetic Mo ions in the Fe sublattice, producing then a dilution effect (–Mo–Fe–Mo–Mo–Mo–Fe–) of the ferromagnetic interactions among Fe ions, which would counterbalance the enhancement due to AFM nearest-neighbour interactions (–Mo–Fe–Fe–Fe–Mo–Fe–). Consequently, it can be argued that if additional nearest-neighbour antiferromagnetic Fe–Fe interactions could be created *without* diluting the Fe sublattice, an enhancement of the ferromagnetic coupling, and thus of the Curie temperature, should be expected. This situation can be achieved in $A_2Fe_{1+x}Mo_{1-x}O_6$ samples in which the Fe:Mo ratio is not 1:1 but $1+x$:$1-x$ ($x < 1$).

The goal of this paper is to provide evidence of the effectiveness of this novel strategy to increase the Curie temperature of double perovskites. We will present results corresponding to $A_2Fe_{1+x}Mo_{1-x}O_6$ samples with different amounts of Fe excess (x). In the pristine compound, the valences of Fe and Mo ions differ, so in order to preserve charge neutrality and electron counting upon increasing the Fe concentration, the charge has to be balanced by the partial substitution of divalent A^{2+} ions by a trivalent lanthanide. We recall than in the case of references [4–11], the aim of doping at the A-site of the perovskite structure with a trivalent cation was exactly the opposite, that is, the injection of carriers in the conduction band. Returning to the present series, an appropriate choice is the substitution of Ca^{2+} by Nd^{3+}; because of their virtually identical ionic radii ($r_{Nd^{3+}} = 1.11$ Å and $r_{Ca^{2+}} = 1.12$ Å), the steric effects associated to the substitution would be minimized. Therefore, we have explored the properties of $(Ca_{1-y}Nd_y)_2Fe_{1+x}Mo_{1-x}O_6$ oxides.

We should point out that achieving an exact charge balance (by means of adequately adapting the Ca/Nd ratio) when the Fe content is increased implies having a precise knowledge of the formal valences of Fe^{m+} and $Mo^{m'+}$ ions. It is well known that Fe and Mo in double perovskites present mixed valence 3+/2+ and 5+/6+ states, respectively [18–20]. For instance, in the particular case of Ca_2FeMoO_6, the measured isomer shift of Fe nuclei in Mössbauer experiments is found to be around $\sim$0.68 mm s^{-1} [20]; this value is intermediate between typical values for Fe^{3+} ($\sim$0.5 mm s^{-1}) [21] and Fe^{2+} ($\sim$1.2 mm s^{-1}) [21], and corresponds to a formal Fe valence of $\sim$2.7+. Therefore, to overcome this ambiguity, two limiting scenarios that would keep charge neutrality in the cases of Fe^{2+}:Mo^{6+} and Fe^{3+}:Mo^{5+} valence configurations have been assumed, and consequently two different series of oxides, with

different compositions, have been prepared: series I, $Nd_{4x}Ca_{2-4x}Fe_{1+x}Mo_{1-x}O_6$, and series II, $Nd_{2x}Ca_{2-2x}Fe_{1+x}Mo_{1-x}O_6$. We therefore expect some electron doping in series I and some hole doping in series II. Indeed, it can be seen that the variation on the electron counting (δn) upon increasing the Fe excess ($x > 0$) in the (Fe_{1+x}:Mo_{1-x}) sublattice corresponds to $\delta n \sim x(> 0)$ for series I and $\delta n \sim -x(< 0)$ for series II.

It will be shown that unbalancing the Fe:Mo ratio from 1:1 to $1 + x$:$1 - x$ dramatically increases the Curie temperature, at a rate of about $\Delta T_C/\Delta x \sim 495$–$460$ K/x ($0 < x < 0.5$) for both series, and we will argue that this is a genuine effect, not attributable to electron/hole doping, and related to the reinforcement of the nearest-neighbour Fe–Fe AFM interactions in the double perovskite structure. Mössbauer data will provide a clear insight into the microscopic evolution of the strength of these interactions with the excess of Fe. The impact of the Fe excess on the magnetization, resistivity, and magnetoresistance will be addressed.

2. Experimental details

$Nd_{4x}Ca_{2-4x}Fe_{1+x}Mo_{1-x}O_6$ (series I) and $Nd_{2x}Ca_{2-2x}Fe_{1+x}Mo_{1-x}O_6$ (series II) ($0 \leqslant x \leqslant 0.25$ and $0 \leqslant x \leqslant 0.5$, respectively) samples were prepared by mixing oxides and carbonates at the appropriate ratio and using the standard solid-state reactions process [11]. Synthesis was performed at 1250 °C in H_2–Ar reducing atmosphere. Structural characterization was done by means of x-ray powder diffraction (Siemens D-5000 diffractometer, Cu Kα1, α2 radiation), at room temperature. Rietveld refinements, performed by means of FullProf software [22], were used to determine the cationic site occupancies. Since the usual definition of antisite concentration (AS) in an 1:1 Fe:Mo lattice—i.e., the number of Fe(Mo) ions misplaced at Mo(Fe) sites—is no longer valid in an unbalanced $1 + x$:$1 - x$ Fe:Mo system, we define here the AS as the number of Mo ions at regular Fe sites, normalized by the total number of Mo atoms. According to this definition, $AS = 0\%$ corresponds to the situation where all Mo ions are placed within one sublattice while the other is fully occupied by Fe ions, and $AS = 50\%$ corresponds to the situation where all Mo and Fe ions are randomly placed within both sublattices. We shall point out that the oxygen stoichiometry was checked by means of neutron powder diffraction in related samples synthesized by the same route [5], finding that the oxygen composition was the nominal within the sensitivity of the technique ($\pm 2\%$). So, it is reasonable to assume that samples reported here also present a nominal oxygen stoichiometry.

The magnetization as a function of the magnetic field was measured at 10 K, by using a commercial Quantum Design superconducting quantum interference device (SQUID) magnetometer. Magnetization versus temperature was recorded using a vibrating sample magnetometer (VSM), from room temperature up to 500 K, under a 0.1 T applied field.

Mössbauer spectra were recorded at 80 K by using a conventional transmission Mössbauer spectrometer with a ^{57}Co/Rh source in the constant acceleration mode. Velocity calibration was done using a 25 μm foil of metallic iron and the isomer shift values are given relative to this standard at room temperature. The full width at half maximum of the calibration foil was 0.32 mm s^{-1}. The spectra were fitted (using program package NORMOS-DIST [23]) by means of a discrete hyperfine field distribution, correlated to a distribution of isomer shifts to describe the asymmetry of the sextets.

3. Results and discussion

X-ray patterns of all samples of series I and II ($Nd_{4x}Ca_{2-4x}Fe_{1+x}Mo_{1-x}O_6$ and $Nd_{2x}Ca_{2-2x}Fe_{1+x}Mo_{1-x}O_6$) were successfully refined using the monoclinic $P2_1/n$ space group, as was previously found for the $Nd_xCa_{2-x}FeMoO_6$ series [11]. In figures 1(a)–(c)

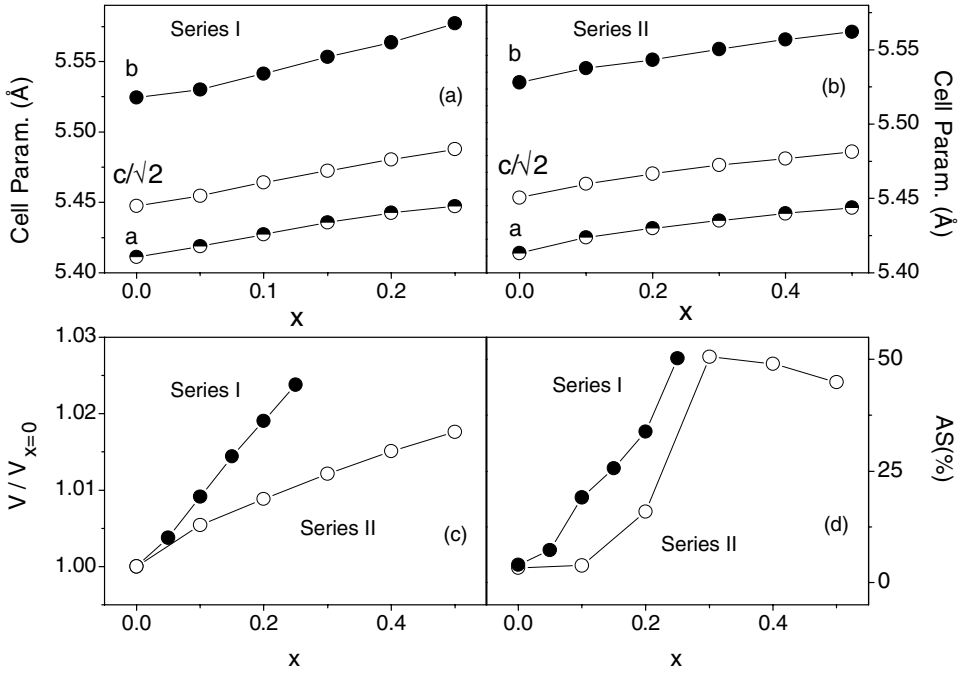

Figure 1. Evolution of the cell parameters as a function of doping for the series (a) $Nd_{4x}Ca_{2-4x}Fe_{1+x}Mo_{1-x}O_6$ (series I) and (b) $Nd_{2x}Ca_{2-2x}Fe_{1+x}Mo_{1-x}O_6$ (series II), respectively. (c), (d) Cell volume and antisite concentration versus x for the same series. The lines are guides to the eye.

we show the evolution of cell parameters and cell volume (normalized by the corresponding values at $x = 0$) for both series. The antisite concentrations are displayed in figure 1(d). In figures 1(a)–(c) it can be appreciated that the unit-cell parameters and the volume of both series expand as the Fe excess (x) increases. From figure 1(c) it is clear that the volume expands at a higher rate for samples of series I than for those of series II. Two effects contribute to cell expansion in series I: a structural one, which is the higher ionic radius of Fe with respect to Mo [24] ($r_{Fe^{2+}} = 0.78$ Å, $r_{Fe^{3+}} = 0.65$ Å $> r_{Mo^{5+}} = 0.61$ Å, $r_{Mo^{6+}} = 0.59$ Å), and the effect of electron injection ($\delta n > 0$) in the conduction band [4, 10, 11]. In contrast, for samples of series II ($\delta n < 0$), the holes that are introduced by the Fe excess should promote a bond shrinking and thus the relative cell expansion must be smaller. Therefore, the faster rise of the cell volume in series I has to be interpreted as a signature of electron doping.

We will focus now on the growth of antisite defects along both series. Figure 1(d) shows that such increase is more pronounced in the case of series I than in series II. In order to rationalize this observation it is necessary to recall that the driving force for the ordering of the M/M′ cations in the metallic sublattice of $A_2MM'O_6$ is related to the difference between their ionic charges. In the particular case of Sr_2FeMoO_6, different local probes such as Mössbauer [20], NMR [25] and photoemission experiments [12] seem to indicate that upon electron doping, injected electrons tend to locate selectively at Mo sites. Hence, the charge difference between Fe and Mo must be lowered, and consequently the driving force for Fe/Mo ordering should be also reduced. Indeed, an enhancement of the antisite concentration has been reported for other electron-doped double perovskites such as $La_xSr_{2-x}FeMoO_6$ [4, 5], $Nd_xSr_{2-x}FeMoO_6$ [10] or $Nd_xCa_{2-x}FeMoO_6$ [11]. A similar reasoning applies here: samples

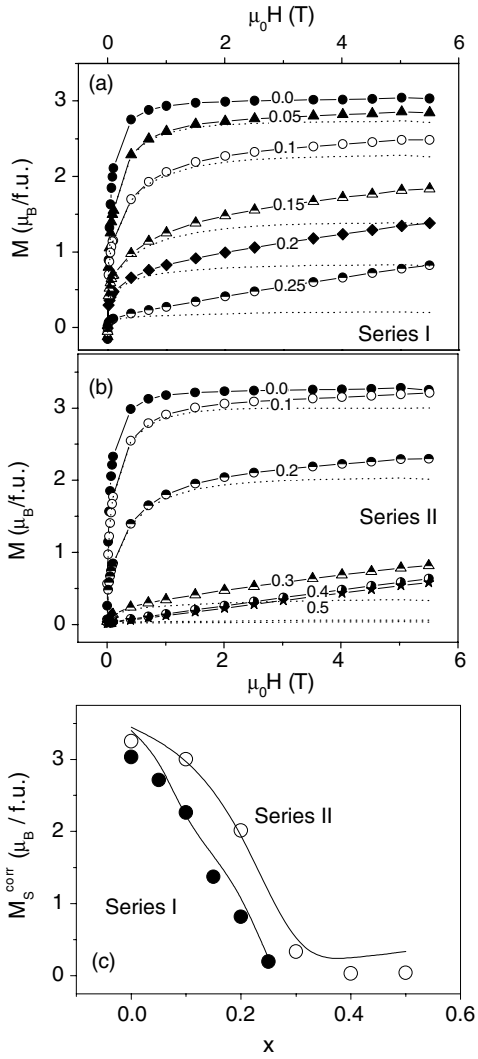

Figure 2. Magnetization as a function of the applied field for the series (a) $Nd_{4x}Ca_{2-4x}Fe_{1+x}Mo_{1-x}O_6$ (series I) and (b) $Nd_{2x}Ca_{2-2x}Fe_{1+x}Mo_{1-x}O_6$ (series II), respectively. The dotted lines are $M(H)$ after the correction for the high-field susceptibility. The continuous lines in (a) and (b) are guides to the eye. Data were taken at 10 K. (c) Experimental (symbols) and estimated (lines) (according to equation (1)) saturation magnetizations for both series.

of series I are electron doped ($\delta n > 0$), and thus we should expect a relatively larger concentration of antisites than for samples of series II.

Figures 2(a) and (b) show the low-temperature (10 K) magnetization as a function of the applied field for series I and II. Inspection of these figures immediately reveals a monotonic reduction of the magnetization upon increasing the content of Fe excess, and the existence of an increasingly large high-field differential susceptibility that can be attributed to paramagnetic Nd ions [10, 11]. Using the procedure described in [10], this contribution to the measured magnetization can be subtracted and the saturation magnetization of the Fe:Mo sublattice (M_S^{corr}) can be extracted. The result of the subtraction is shown as dotted lines in figures 2(a) and (b), and the values of M_S^{corr} are given in figure 2(c). The reduction of M_S^{corr} is due to

two different effects: the introduction of additional Fe ions occupying the spin-down Mo-sublattice, and the increase of antisite defects upon Fe doping [18]. Including both effects, the variation of the saturation magnetization can be described as

$$M_S^{corr} = 4(1-x)(1-2AS)\ \mu_B, \tag{1}$$

where the $(1-x)$ factor accounts for the lowering of the magnetic moment due to the Fe excess introduced into Mo sites, and the factor $(1-2AS)$ takes into account the magnetization reduction produced by antisite disorder [18]. In figure 2(c) we have also plotted the calculated values (lines) of M_S^{corr} using equation (1) and the antisite concentrations values plotted in figure 1(d). It is rewarding to observe that equation (1) describes the experimental data remarkably well.

We will focus now on the evolution of the magnetization as a function of temperature $M(T)$, shown in figures 3(a) and (b) for samples of series I and II, respectively. It can be clearly seen in these figures that the onset of the ferromagnetic state is pushed toward higher temperatures for both series when the Fe content is increased. The Curie temperatures (T_C), determined from the inflection point of the corresponding $M(T)$ curves—the temperature at which dM/dT displays a minimum—are collected in figure 3(c). It is clear that, for both series, T_C is enhanced when an excess of Fe is introduced into the Fe–Mo sublattice. This increase is from ∼360 K for $x = 0$ up to ∼455 K ($x = 0.25$, series I) or to ∼435 K ($x = 0.3$, series II). Therefore, the data in figure 3 show that the presence of Fe excess in irregular Mo sites indeed promotes a remarkable reinforcement of the ferromagnetic ordering, and a concomitant rise of T_C.

It can also be appreciated in figure 3(c), that the initial slope of $T_C(x)$ (dT_C/dx) is somewhat larger for series I ($dT_C/dx \approx 590$ K/x, $0 \leqslant x \leqslant 0.1$) than for series II ($dT_C/dx \approx 365$ K/x, $0 \leqslant x \leqslant 0.2$).[4] The difference of dT_C/dx observed in both series is due to the fact that, associated to the Fe excess, the samples also differ in their carrier concentration. Indeed, for series I the electron doping ($\delta n > 0$) contributes to raising the dT_C/dx rate, while in the case of series II the hole injection ($\delta n < 0$) should produce the opposite effect [26]. We have previously shown [11] that in the electron-doped $Nd_xCa_{2-x}FeMoO_6$ series, T_C grows at a rate of about 1.9 K/%Nd, or equivalently 95 K/e^- (where e^- refers to the injected electrons). Therefore, it can be inferred that the contribution of electron doping to the T_C rise in series I is of about ∼95 K/e^- or ∼95 K/x. Similarly, the injection of holes present in series II would induce a T_C lowering, which, in the case of a symmetrical behaviour, would correspond to a reduction of ∼−95 K/x. Hence, after the subtraction of the carrier variation effect from the overall T_C versus x slopes, it turns out that the corrected values are $\approx (590-95)$K/$x \approx 495$ K/x for series I, and $\approx (365+95)$K/$x \approx 460$ K/x for series II. It thus follows that the growth rate of T_C, including *only* the contribution of the Fe excess, is very similar in both series. Finally, we notice in figure 3(c) that above some critical composition ($x > 0.3$ for series II), T_C gradually decreases. This observation reflects the increasing contribution of the AFM Fe–Fe bonds, which should finally overcome the ferromagnetic Fe–O–Mo paths, as the Fe concentration rises. Since the magnetic moments of the Fe ions couple antiferromagnetically to nearest neighbours via a superexchange mechanism, a ferrimagnetic-like structure should be formed, with reduced magnetic moment and stronger overall ferromagnetic interactions. However, as x increases further, the interactions gradually transform from ferromagnetic to antiferromagnetic. Therefore, in agreement with experimental data, a reduction of T_C must be observed above a critical x-value.

[4] Samples of series I and II were prepared in different batches. The differences in T_C-values of the $x = 0$ samples of series I and II reflects the extreme sensitivity of the properties of double perovskites on subtle details of the synthesis conditions.

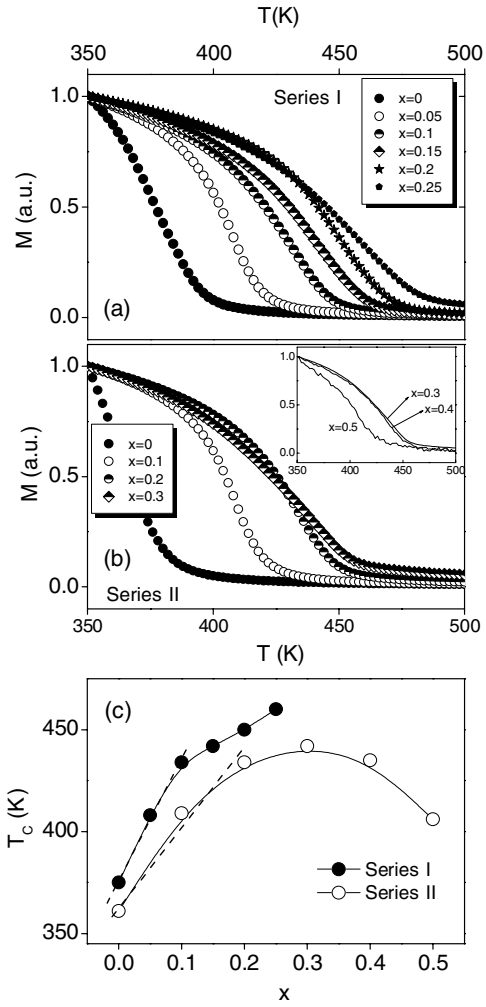

Figure 3. Evolution of the magnetization as a function of the temperature (a 0.1 T field was used) for the series (a) $Nd_{4x}Ca_{2-4x}Fe_{1+x}Mo_{1-x}O_6$ (series I) and (b) $Nd_{2x}Ca_{2-2x}Fe_{1+x}Mo_{1-x}O_6$ (series II), respectively. (c) Curie temperature (as explained in the text) versus x for both series. The dashed line shows a linear fit to the initial dT_C/dx slope, while the continuous lines are guides to the eye. For the sake of clarity, the curves shown in (b) were split between the main panel and the inset.

In order to monitor the suggested modification of the strength of the Fe–Fe magnetic coupling, we have performed transmission Mössbauer experiments on some of the samples. In figure 4 we present the Mössbauer spectra of selected samples of series II, recorded at 80 K, i.e., well below the Curie temperature. A well-defined sextet is apparent for all samples. Inspection of these spectra immediately reveals that the hyperfine splitting becomes progressively larger on increasing the Fe contents. Since the hyperfine field measures the Weiss molecular magnetic field, the data in figure 4 indicate that the molecular field, and thus the magnetic interactions, strengthen when the Fe content is increased.

The spectrum of the $x = 0$ sample (top), corresponding to the pristine Ca_2FeMoO_6, is very similar to the earlier reported spectra [19, 20]. Greneche *et al* [19] fitted a similar spectrum

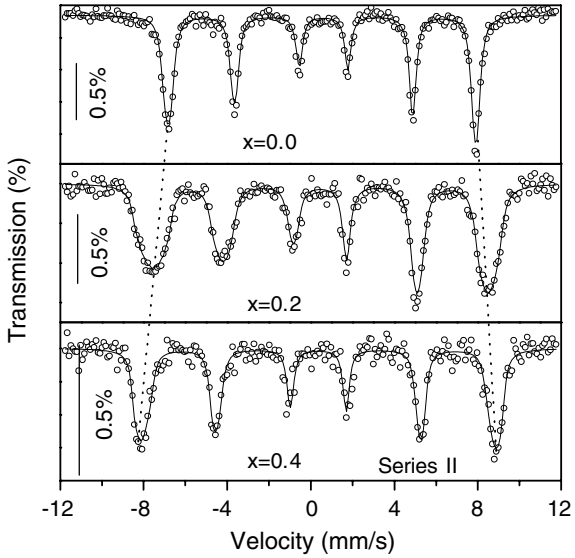

Figure 4. Mössbauer spectra, taken at 80 K, for selected samples corresponding to $Nd_{2x}Ca_{2-2x}Fe_{1+x}Mo_{1-x}O_6$ series. Data (open symbols) were fitted by using a distribution of hyperfine fields, as explained in the text. The dotted lines show the evolution of the hyperfine splitting on increasing the Fe content.

using three different sextets that were attributed to Fe ions at regular positions, antisites and antiphase boundaries. For the purpose of this paper, it is more appropriate to describe the spectra of all samples in terms of a distribution of hyperfine fields reflecting the different surroundings of the Fe ions in the $A_2Fe_{1+x}Mo_{1-x}O_6$ lattice. Notice that the number of Fe neighbouring ions ($n = 0$–6) for a given Fe ion depends on both the antisite (AS) and the Fe(x) excess concentration; the relative probability $P(n)$ of an Fe being surrounded by n nearest Fe neighbours can be evaluated by means of the following expression:

$$P(n) = \binom{6}{n} pq^n(1-q)^{6-n} + \binom{6}{n} qp^n(1-p)^{6-n} \tag{2}$$

where p and q are the probabilities of an Fe being placed on each of the two Wyckoff positions corresponding to the different Fe and Mo sublattices. p and q can be easily calculated from x and AS, or, equivalently, from the corresponding crystallographic site occupations.

It should be expected that the hyperfine field (HF) acting on the different Fe nuclei would depend on n, and, correspondingly, the spectra must contain contributions from all these configurations and thus—at least seven—different $HF_n(n = 0–6)$ fields should exist. Their relative weight into the spectra would be proportional to $P(n)$. As a consequence, we have used a distribution of hyperfine fields [HF_n ($n = 0–6$)] with different intensities to fit all spectra. The hyperfine fields are assumed to be given by $HF_n(x) = HF_0(x) + n\Delta HF(x)$. The fit of the spectra provides the values of $HF_0(x)$ and $\Delta HF(x)$, and therefore of the $HF_n(x)$-values, the corresponding relative intensities $A_n(x)$, and the isomer shift values $IS_n(x)$; $IS_n(x) = IS_0(x) + n\Delta IS(x)$, where IS_0 and $\Delta IS(x)$ are extracted from the fits. To minimize the fitting parameters, the full width at half maximum [$\Gamma_n(x)$] of the resonances has been assumed to be $\Gamma = 0.35$ mm s^{-1} for $x = 0, 0.1, 0.3, 0.4$, and $\Gamma = 0.45$ mm s^{-1} for $x = 0.2$. From the values of $HF_n(x)$ and $A_n(x)$, we have evaluated the weighted hyperfine field mean values [$\langle HF(x)\rangle = \sum A_n(x)HF_n(x)/\sum A_n(x)$], and the standard deviations of the distributions

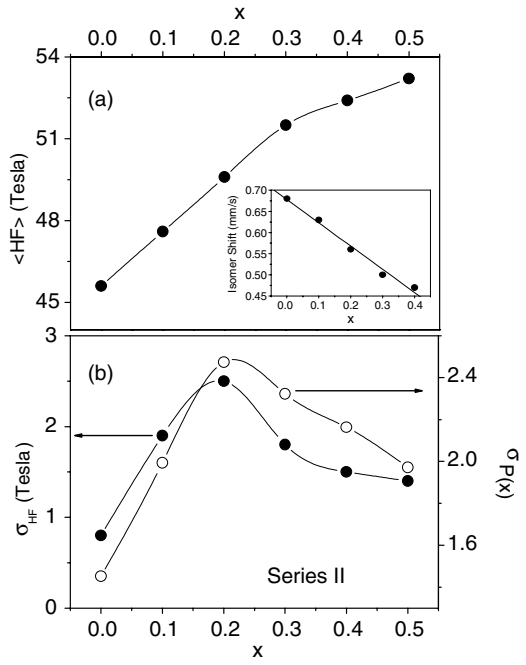

Figure 5. (a) Evolution of the mean hyperfine field $\langle \mathrm{HF}(x) \rangle$ (main panel) and mean isomer shift $\langle \mathrm{IS}(x) \rangle$ (inset) of samples belonging to the $Nd_{2x}Ca_{2-2x}Fe_{1+x}Mo_{1-x}O_6$ series. (b) Standard deviation of the hyperfine width distribution ($\sigma_{\mathrm{HF}}(x)$) and width of the calculated probability distribution ($\sigma_{P(x)}$) corresponding to the same samples. The lines are guides to the eye.

($\sigma_{\mathrm{HF}}(x)$). The mean isomer shift values ($\langle \mathrm{IS}(x) \rangle$) have been evaluated similarly. Figure 5(a), where we present the evolution of $\langle \mathrm{HF}(x) \rangle$ and $\langle \mathrm{IS}(x) \rangle$ (main panel and inset, respectively), reveals two important observations. First, the hyperfine field gradually increases with x. We note that whereas for the pristine compound $\langle \mathrm{HF}(0) \rangle \approx 45$ T, in agreement with reported values [20], the hyperfine field increases up to $\langle \mathrm{HF}(0.4) \rangle \approx 52$ T for $x = 0.4$. We note that for this heavily doped sample, the HF value is, as expected, similar to what is reported in ferric oxides such as Fe_2O_3 [27]. Second, the mean isomer shift value—measuring the s-electron density at the nuclei of Fe ions—gradually decreases from $\langle \mathrm{IS}(0) \rangle \approx 0.68$ mm s^{-1} down to $\langle \mathrm{IS}(0.4) \rangle \approx 0.47$ mm s^{-1} (see the inset in figure 5(a)). These observations are in agreement with the detailed analysis performed by Greneche *et al* in the pristine sample [19]; it was shown that Fe ions at irregular positions have smaller isomer shift values. Therefore, our observation of a gradual lowering of the isomer shift $\langle \mathrm{IS}(x) \rangle$ simply reflects the increasing weight in the Mössbauer spectra of Fe ions at irregular positions.

In figure 5(b) we include the standard deviation of the hyperfine width distribution $\sigma_{\mathrm{HF}}(x)$ (full symbols), reflecting the trend that was already visible in the raw spectra of figure 4; namely that on increasing x, the width of the Mössbauer lines increases and reaches a maximum at about $x = 0.2$–0.3, before reducing again for larger x-values. This trend is reflecting the fact that for $x = 0$ (and $AS = 0$) all Fe ions are equivalent and for all of them $n = 0$, thus $P(n)$ is largely peaked at $n = 0$ (for $x = 0$). A similar situation holds for the largest x, where most of Fe ions should have Fe as nearest neighbours, thus implying that the $P(n)$ probability should have a pronounced peak at $n = 6$ (for $x \approx 1$). At intermediate x-values a large number of different configurations should be present and thus $P(n)$ is largely spread over

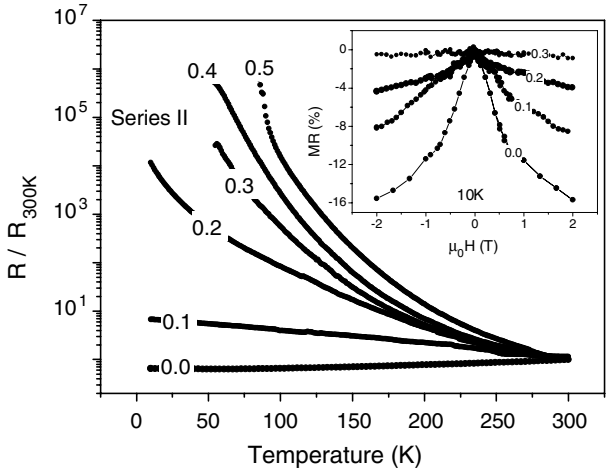

Figure 6. Main panel: normalized (300 K) resistivity versus temperature for $Nd_{2x}Ca_{2-2x}Fe_{1+x}Mo_{1-x}O_6$ samples. Inset: evolution of the magnetoresistance (at 10 K) for the same samples. The lines are guides to the eye.

several intermediate n-values. The width of the probability distribution for each compound ($\sigma_{P(x)}$), shown in figure 5(b) (open symbols), has been computed from the expression

$$\sigma^2_{P(x)} = \langle n^2 \rangle - \langle n \rangle^2 = \sum_n P(n)n^2 - \left[\sum_n P(n)n\right]^2 \tag{3}$$

where $P(n)$ was calculated according to equation (2). Figure 5(b) clearly shows that both the standard deviation of the hyperfine width distribution [$\sigma_{HF}(x)$], and the width of the calculated probability distribution [$\sigma_{P(x)}$] exhibit a similar trend when the Fe content is increased. It thus follows that the observed line broadening in Mössbauer spectra for intermediate x-values is a consequence of the different surroundings for Fe nuclei and its dependence on x.

We turn now to the transport properties. The main panel of figure 6 shows the evolution of the normalized resistivity (at 300 K) as a function of the temperature for samples of series II. The gradual substitution of Fe–O–Mo bonds by Fe–O–Fe paths is expected to suppress the metallic conductivity of the pristine sample (Ca_2FeMoO_6). Indeed, it is observed that an insulating-like behaviour develops when Fe doping takes place. Furthermore, the $x = 0.5$ room-temperature resistivity is found to be three orders of magnitude higher than that corresponding to the $x = 0$ sample. A similar behaviour has also been found for samples belonging to series I (not shown here). The inset of figure 6 shows the evolution of the magnetoresistance (MR, measured at 10 K) for series II. The MR is found to decrease when the Fe content is increased, presumably due to the suppression of Fe–O–Mo bonds upon doping, which may impact on the half-metallic character of these double perovskites.

4. Summary and conclusion

We have reported here that the ferromagnetic Curie temperature of double perovskites A_2FeMoO_6 can be substantially increased by reinforcing the nearest-neighbour interactions. This is achieved by introducing magnetic ions (Fe) in the Mo sublattice. The success of this strategy relies on the fact that in the Fe:Mo (1:1) structure, Fe at Mo positions locally reinforces the magnetic interactions but this effect competes with the dilution of the Fe–Fe interaction

at regular positions. This difficulty is overcome when an excess of Fe is introduced in the structure. Mössbauer experiments have provided a clear insight into the microscopic origin of the enhanced magnetic interactions. Unfortunately, the enhancement of the Curie temperature is accompanied by a reduction of the overall magnetization, an increase of the resistivity, and a loss of magnetoresistance. We argued that this behaviour is related to disorder induced by Fe excess.

Acknowledgments

Financial support by the CICYT of the Spanish Government (projects MAT2002-04551-C03 and MAT2003-07483-C02). CF acknowledges financial support from MEC (Spanish government).

References

[1] Kobayashi K I, Kimura T, Sawada H, Terakura K and Tokura Y 1998 *Nature* **395** 677
[2] Tovar M, Causa M T, Butera A, Navarro J, Martínez B, Fontcuberta J and Passeggi M C G 2002 *Phys. Rev.* B **66** 024409
[3] Kanamori J and Terakura K 2001 *J. Phys. Soc. Japan* **70** 1433
[4] Navarro J, Frontera C, Balcells L, Martínez B and Fontcuberta J 2001 *Phys. Rev.* B **64** 092411
[5] Frontera C, Rubi D, Navarro J, García-Muñoz J L, Fontcuberta J and Ritter C 2003 *Phys. Rev.* B **68** 012412
[6] Sánchez D, Alonso J A, García-Hernandez M, Martínez-Lope M J, Casais M T and Martínez J L 2003 *J. Mater. Chem.* **13** 1771
[7] Serrate D, de Teresa J, Blasco J, Ibarra M, Morellon L and Ritter C 2002 *Appl. Phys. Lett.* **80** 4573
[8] Lindén J, Shimada T, Motohashi T, Yamauchi H and Karppinen M 2004 *Solid State Commun.* **129** 129
[9] Yang H M, Lee W Y, Han H, Lee B W and Kim C S 2003 *J. Appl. Phys.* **83** 10
[10] Rubi D, Frontera C, Nogués J and Fontcuberta J 2004 *J. Phys.: Condens. Matter* **16** 3173
[11] Rubi D, Frontera C, Fontcuberta J, Wojcik M, Jedryka E and Ritter C 2004 *Phys. Rev.* B **70** 094405
[12] Navarro J, Fontcuberta J, Izquierdo M, Avila J and Asensio M C 2004 *Phys. Rev.* B **69** 115101
[13] Ogale A S, Ogale S B, Ramesh R and Venkatesan T 1999 *Appl. Phys. Lett.* **75** 537
[14] Frontera C and Fontcuberta J 2004 *Phys. Rev.* B **69** 014406
[15] Alonso J L, Fernández L A, Guinea F, Lesmes F and Martín-Mayor V 2003 *Phys. Rev.* B **67** 214423
[16] Solovyev I V 2002 *Phys. Rev.* B **65** 144446
[17] Navarro J, Nogués J, Muñoz J S and Fontcuberta J 2003 *Phys. Rev.* B **67** 174416
[18] Balcells L L, Navarro J, Bibes M, Roig A, Martínez B and Fontcuberta J 2001 *Appl. Phys. Lett.* **78** 781
[19] Greneche J M, Venkatesan M, Suryanaryanan R and Coey J M D 2001 *Phys. Rev.* B **63** 174403
[20] Yasukawa Y, Lindén J, Chan T S, Liu R S, Yamauchi H and Karppinen M 2004 *J. Solid State Chem.* **177** 2655
[21] Vértes A, Korecz L and Burhuer K 1979 *Mössbauer Spectroscopy* (New York: Elsevier Scientific) p 47, Table I.5
[22] Rodríguez Carvajal J 1993 *Physica* B **192** 55
[23] Brand R A 1987 *Nucl. Instrum. Methods* B **28** 398
[24] Shannon R D 1976 *Acta Crystallogr.* A **32** 751
[25] Wojcik M, Jedryka E, Nadolski S, Navarro J, Rubi D and Fontcuberta J 2004 *Phys. Rev.* B **69** 100407
[26] Kim J, Sung J G, Yang H M and Lee B W 2005 *J. Magn. Magn. Mater.* **290/291** 1009
[27] Shirane G, Cox D E and Ruby S L 1962 *Phys. Rev.* **125** 1158